Acta Pharmacologica Sinica

www.nature.com/aps

ARTICLE

MK2206 attenuates atherosclerosis by inhibiting lipid accumulation, cell migration, proliferation, and inflammation

Ya-qin Tang[1], Zhi-wei Li[1], Yu-fan Feng[1], Hong-qin Yang[1], Cui-liu Hou[1], Chi Geng[1], Pei-ran Yang[1], Hong-mei Zhao[1] and Jing Wang[1]

Cardiovascular disease is a common comorbidity in patients with cancer, and the main leading cause of noncancer-related deaths in cancer survivors. Considering that current antitumor drugs usually induce cardiovascular injury, the quest for developing new antitumor drugs, especially those with cardiovascular protection, is crucial for improving cancer prognosis. MK2206 is a phase II clinical anticancer drug and the role of this drug in cardiovascular disease is still unclear. Here, we revealed that MK2206 significantly reduced vascular inflammation, atherosclerotic lesions, and inhibited proliferation of vascular smooth muscle cell in ApoE$^{-/-}$ mice in vivo. We demonstrated that MK2206 reduced lipid accumulation by promoting cholesterol efflux but did not affect lipid uptake and decreased inflammatory response by modulating inflammation-related mRNA stability in macrophages. In addition, we revealed that MK2206 suppressed migration, proliferation, and inflammation in vascular smooth muscle cells. Moreover, MK2206 inhibited proliferation and inflammation of endothelial cells. The present results suggest that MK2206, as a promising drug in clinical antitumor therapy, exhibits anti-inflammatory and antiatherosclerotic potential. This report provides a novel strategy for the prevention of cardiovascular comorbidities in cancer survivors.

Keywords: atherosclerosis; Akt; MK2206; inflammation; cholesterol efflux

Acta Pharmacologica Sinica (2022) 43:897–907; https://doi.org/10.1038/s41401-021-00729-x

INTRODUCTION

The prevalence of cancer and its associated comorbidities is one of the greatest challenges for the healthcare system [1, 2]. Cardiovascular disease (CVD) is a common comorbidity in cancer patients, implicated in poor patient prognosis and tumor progression [3]. Previous studies suggest that CVD is the main leading cause of noncancer-related deaths in cancer survivors and the major risk of adverse cardiovascular events in anticancer therapy trial participants [4, 5], making cardiovascular dysfunction one of the major concerns for anticancer therapy. The cardiovascular toxicity of current therapeutic drugs for cancer [6] prompted us to find a new drug effective for both cancer and CVD. Atherosclerosis is the pathological basis of CVD and the leading cause of cardiovascular events. Thus, we searched for an effective therapy that targeted common signaling pathways in cancer and atherosclerosis.

Multiple studies suggest that Akt plays an important role both in the pathogenesis and progression of atherosclerosis and cancer [7, 8], exposing it as a potential common target for atherosclerosis and cancer. MK2206 is a highly selective allosteric inhibitor of Akt in phase II studies for patients with refractory renal cell carcinoma [9], relapsed or refractory lymphoma [10], and advanced thoracic malignancies [11]. Compared to other pan-Akt inhibitors, such as upstream inhibitors and ATP-binding pocket inhibitors, the allosteric inhibitor is a new strategy for alleviating off-target toxicity. In addition, MK2206 inhibits all three Akt kinases isoforms (Akt1, Akt2, and Akt3), with specificity and acceptable toxicities [12]. As a promising anticancer agent with broad clinical applications and great advantages, the role of MK2206 in atherosclerosis remains unclear.

Atherosclerotic CVD leads the common causes of death worldwide [13]. The pathogenesis of atherosclerosis involves endothelial dysfunction [14], macrophage foam cell formation [15], vascular smooth muscle cell (VSMC) migration and proliferation [16], and chronic inflammatory processes of the arterial wall among others [15]. At the molecular level, scavenger receptors CD36 and scavenger receptor-A (SR-A) are responsible for the internalization of oxidized low-density lipoproteins (oxLDL), which mediates macrophage lipid uptake [17]. The ATP-binding cassette transporter A1 and G1 (ABCA1 and ABCG1) transport cholesterol from the macrophage to high-density lipoprotein (HDL) [18], which then delivers cholesterol to the liver through apolipoprotein A1 (ApoA1) via scavenger receptor class B type I (SR-BI) [19], thereby promoting macrophage cholesterol efflux. The imbalance between macrophage lipid uptake and cholesterol efflux leads to foam cell formation. Matrix metalloproteinases (MMPs) are a family of proteolytic enzymes that degrade extracellular matrix and mediate vascular remodeling [20]. MMP2 and MMP9 are the most extensively studied MMPs in vascular disease, reported to facilitate cell migration and proliferation [21], and are associated with the stability of atherosclerotic vulnerable plaque [22]. In addition to the above pathological mechanisms, inflammation plays an essential role in atherosclerosis. Intracellular adhesion molecule 1 (ICAM1), vascular cell adhesion molecule 1 (VCAM1),

[1]State Key Laboratory of Medical Molecular Biology, Institute of Basic Medical Sciences, Chinese Academy of Medical Sciences, Department of Pathophysiology, Peking Union Medical College, Beijing 100005, China
Correspondence: Hong-mei Zhao (hongmeizhao@ibms.pumc.edu.cn) or Jing Wang (wangjing@ibms.pumc.edu.cn)

Received: 28 February 2021 Accepted: 27 June 2021
Published online: 27 July 2021

P-selectin, and E-selectin are associated with endothelial activation and damage, promotes inflammatory response and atherosclerosis [23, 24], interleukin-1β (IL-1β), IL-6, C–C motif chemokine ligand 2 (CCL2) and tumor necrosis factor α (TNF-α) levels are generally increased in patients with atherosclerosis, while therapeutic interventions targeting inflammation factors expressed in various cells can prevent the disease progression [25–27]. Interestingly, Akt regulates many of these atherogenesis-associated processes, such as macrophage lipid uptake [28], VSMC migration [29], and inflammation [30]. However, whether the Akt inhibitor MK2206 could affect the progress of atherosclerosis through modulation of these mechanisms remains unknown.

Here, we first measured the lipid accumulation and inflammatory response in ApoE$^{-/-}$ mice to determine the protective role of MK2206 in vivo. Subsequently, we investigated the effects of MK2206 on macrophage lipid accumulation, VSMC migration and proliferation, endothelial damage and proliferation, and the regulation of inflammatory response in macrophages, VSMCs, and endothelial cells. In conclusion, we used a range of in vivo and in vitro approaches to demonstrate the protective role of MK2206 in CVD.

MATERIALS AND METHODS

Cell culture and treatment

Human aortic VSMCs (HASMCs), human umbilical vascular endothelial cells (HUVEC), and mouse leukemic monocyte/macrophage cell line (Raw264.7) were purchased from the National Infrastructure of Cell Line Resource, China. HASMCs were cultured in smooth muscle cell medium (SMCM, Sciencell, CA, USA) containing 2% fetal bovine serum (FBS), 1% smooth muscle cell growth supplement (SMCGS, Sciencell), and 1% penicillin/streptomycin solution (Sciencell). HUVECs were cultured in endothelial cell medium (Sciencell) containing 5% FBS (Sciencell), 1% endothelial cell growth supplement (ECGS, Sciencell), and 1% penicillin/streptomycin solution (Sciencell). Raw264.7 cells were cultured in Dulbecco's modified Eagle's medium (DMEM, Gibco, NY, USA) containing 10% FBS (Gibco), 100 IU/mL penicillin, and 100 g/mL streptomycin (Gibco). All cells were cultured in a humidified incubator at 37 °C with 5% CO_2.

For induction of inflammation, Raw264.7, HASMC, and HUVEC cells were pretreated with MK2206 (100 nM) for 30 min and incubated with LPS (100 ng/mL) or oxLDL (100 μg/mL, Yiyuan Biotech, Guangzhou, China) for the indicated lengths of time. Subsequently, cell culture supernatant and cells were collected, the supernatant was analyzed by enzyme-linked immunosorbent assay (ELISA) to measure cytokine secretion, and cells processed for RNA extraction.

Animals

A total of 17 male ApoE$^{-/-}$ (C57BL/6J) mice aged 8 weeks old were obtained from Vital River Laboratory Animal Technology Co. Ltd. (Beijing, China), and maintained under specific-pathogen-free conditions. All experimental mice were kept in constant temperature (22–25 °C) and humidity (50%–60%) with a 12/12 h light-dark cycle. Mice were randomly divided into a normal chow diet (control group, $n = 5$) or a high-fat diet (HFD). HFD-fed mice were randomly assigned to HFD group ($n = 6$) and HFD + MK2206 group ($n = 6$) for a further 8-week treatment. Mice from HFD + MK2206 group were intraperitoneally injected with MK2206 at a dose of 4 mg · kg^{-1} · d^{-1}, mice from HFD group were injected with an equal volume of saline (containing 0.1% DMSO), and mice from normal chow diet group were injected with an equal volume of saline as a negative control. All animal experimental procedures were approved by the Animal Care and Use Committee of Peking Union Medical College according to institutional guidelines for animal ethics.

Cell viability assay

Raw264.7, VSMC, and HUVEC cells were cultured in 96-well plates to 80% confluence, then incubated with different concentrations of MK2206 for 24 h. Cell viability was detected with Cell Counting Kit-8 (CCK-8) (Dojindo, Shanghai, China) according to the manufacturer's instruction. Briefly, after MK2206 treatment, cells were incubated with 10 μL CCK-8 solution at 37 °C for 2 h and the absorbance of each well at 450 nm was measured with an Epoch microplate spectrophotometer (BioTek, VT, USA).

Oil Red O staining

Raw264.7 cells were cultured in six-well plates to 80% confluence, and then treated with 100 nM MK2206 (Selleck Chemicals, TX, USA) for 30 min before stimulation with 100 μg/mL oxLDL for 24 h. Fresh tissues from mice were embedded in OCT matrix (Leica, Wetzlar, Germany), and sectioned with the cryostat (Leica 3050S) at 6 μm/slice. Oil Red O staining was conducted using Oil Red O stain kit (Solarbio, Beijing, China), according to the manufacturer's instruction. In brief, Raw264.7 cells or OCT-embedded sections were fixed with 4% paraformaldehyde for 20 min and then rinsed with distilled water three times. Next, cells or sections were immersed with 60% isopropanol for 5 min, followed by staining with fresh ORO solution for 20 min at room temperature. After discarding this solution, cells and sections were rinsed three times with distilled water. After final rinsing, hematoxylin (Mayer) solution was added onto cells and sections for 1 min, and cells and sections were rinsed again three times with distilled water. Images were captured under microscope (Nikon, Tokyo, Japan), and quantification of staining area was evaluated by Image-Pro Plus software after using computer-assisted image quantification system.

Analysis of Dil-oxLDL uptake

Raw264.7 cells were cultured in 12-well plates for 24 h, monolayer cells were treated with 100 nM MK2206 for 30 min before 10 μg/mL dioctadecyl-3,3,3,3-tetramethylindocarbocyanine-oxLDL (Dil-oxLDL, Invitrogen, CA, USA) was supplemented into culture media. After a 6-h incubation, cells were washed twice with phosphate buffer saline (PBS) and imaged with an inverted fluorescence microscope (Nikon). The uptake of Dil-oxLDL was measured by flow cytometry (BD Biosciences, CA, USA), the mean fluorescence intensity (MFI) was calculated from at least 30,000 events of each sample.

Cholesterol efflux assay

Cholesterol efflux assay was conducted as described in previous studies [31, 32], with minor modifications. Briefly, Raw264.7 cells were cultured in 12-well plates for 24 h, the cells were treated with 100 nM MK2206 for 30 min before incubating with 5 μM 22-(N-[7-nitrobenz-2-oxa-1,3-diazol-4-yl] amino)−23,24-bisnor-5-cholen-3β-ol (NBD cholesterol, Invitrogen) in phenol red-free DMEM medium for 4 h at 37 °C. After incubation, the cells were washed with PBS three times and treated with 15 μg/mL ApoA1 (Sigma-Aldrich, MO, USA) or 50 μg/mL HDL (Yiyuan Biotech). Subsequently, the culture medium was collected, and loaded cells were lysed with 0.1% Triton X-100 for 15 min at room temperature. The fluorescence intensity (FI) of culture medium and cell lysate was measured in a black polystyrene 96-well plate with an Epoch microplate spectrophotometer at the wavelength of 469 nm excitation and 537 nm emission. The cholesterol efflux (%) was calculated as follows: Efflux (%) = (culture medium FI: (culture medium FI + cell lysate FI)) × 100.

Transwell migration assay

VSMCs were resuspended in serum-free SMCM, seeded in the upper chamber of 24-well transwell inserts (Corning, NY, USA) and 400 μL of SMCM containing 2% FBS was added to the lower chamber. After 30 min incubation, 100 nM MK2206 was added to the medium in the upper chamber and PDGF-BB (20 ng/mL) to the lower chamber, and the cells were incubated for 24 h at 37 °C.

Subsequently, cells were fixed and permeabilized with methanol for 10 min. Cells were then stained with 0.1% crystal violet for 20 min. Finally, cells on the inside membrane of the upper chamber were carefully removed with a cotton swab, while cells on the outside membrane (migration cells) were imaged using a Nikon inverted microscope. Five random fields per well were captured and the number of migrated cells was counted.

Wound healing assay

The wound healing assay was performed to assess cell migration. VSMCs were cultured in six-well plates for 24 h, the monolayer was scratched using 200 μL sterile pipette tips, and immediately washed three times with PBS. Cells were then stimulated with 100 nM MK2206 for 30 min before supplementing with PDGF-BB (20 ng/mL) for subsequent 24 h incubation. After incubation, cells were imaged using a Nikon inverted microscope. Four fields per well were captured and the migration area was measured by Image-Pro Plus software.

Proliferation assay

Cell proliferation assay was measured by CCK-8 kit according to the manufacturer's instruction. In brief, cells (3×10^3 cells/well) were cultured in 96-well plates and treated with MK2206 for 0, 24, 48, and 72 h, respectively. Subsequently, 10 μL CCK-8 solution was added to each well and incubated for 2 h at 37 °C. Absorbance at 450 nm was read with Epoch microplate spectrophotometer.

mRNA stability assay

Raw264.7, HUVEC, and VSMC cells were cultured in six-well plates to 80% confluence, then cells were treated with MK2206 (100 nM) for 5 h before incubating with actinomycin D for the indicated time points. The total RNA was isolated and subjected to quantitative real-time polymerase chain reaction (RT-qPCR) to analyze mRNA stability.

RNA preparation and RT-qPCR

Total RNA of cells was isolated by using TRIzol reagent (Invitrogen) according to the manufacturer's instructions. Purity and concentration of RNA were quantified at 260 nm wavelength with Nanodrop (Thermo Fisher Scientific, Waltham, USA). According to the manufacturer's instructions of FastKing RT Kit (TianGen, Beijing, China), 1 μg of total RNA was prepared as a template for the first-strand cDNA synthesis of reverse-transcription polymerase chain reaction. Briefly, the first reaction procedure was performed at 42 °C for 3 min, second reaction procedure was performed at 42 °C for 15 min, 95 °C for 30 min, then chilled on ice.

The RT-qPCR was performed by using a 2x Taq master mix (TianGen, Beijing, China) in the CFX96 Touch™ System (Bio-Rad, CA, USA). The specific primers used in this study were designed by Primer5 software (Supplementary Materials Table 1). The program of qPCR was conducted as follows: 95 °C for 30 s, followed by 40 cycles of 95 °C for 10 s and 60 °C for 30 s, a melting curve of 65–95 °C with an increment of 0.5 °C for 5 s per cycle. Final data were calculated by using $2^{-\Delta\Delta Ct}$ method, and relative gene mRNA expression levels were normalized to that of β-actin.

Cytokine assays by ELISA

Cytokine levels in cell culture supernatant or mouse plasma were measured by ELISA (R&D Systems, MN, USA), according to the manufacturer's instructions.

Western blot analysis

Cells were lysed in RIPA buffer for 30 min, cell lysates were collected. After that, total protein concentration was measured by BCA Protein Assay Kit (Thermo Scientific, Waltham, USA). Twenty micrograms of the protein sample was separated on 10% sodium dodecyl sulfate–polyacrylamide gel electrophoresis and then transferred to preactivated polyvinylidene difluoride membrane (Millipore, Billerica, USA). The membrane was then blocked in Tris-buffered saline-Tween (TBST) containing 5% skim milk for 1 h at room temperature, followed by overnight incubation with primary antibody (Supplementary Materials Table 2) at 4 °C. After that, the membrane was washed with TBST and incubated with secondary antibody for 1 h at room temperature. Membranes were incubated with ECL reagents (Thermo Scientific) for chemiluminescence detection, and the immunoreactivity was measured with Tanon Chemiluminescence/Fluorescence Image Analysis System (Tanon, Shanghai, China). The relative intensity of protein bands was quantified with Image-Pro Plus software.

Immunohistochemical (IHC) and immunofluorescent staining

IHC and immunofluorescent staining was performed as previous described [33, 34] with minor modification. Briefly, OCT-embedded frozen sections of the arch were fixed in precooled acetone for 10 min and then washed three times in PBS. Subsequently, sections were added 3% hydrogen peroxidase to block endogenous peroxidase activity for 15 min followed by three washes in PBS for IHC staining. Sections were then blocked with goat serum for 30 min, and then incubated overnight with primary antibodies (Supplementary Materials Table 3) diluted in the goat serum solution at 4 °C. After three washes in PBS, sections were incubated with secondary antibody for 30 min at room temperature. Images were captured using Nikon microscopy. The staining area was measured using a computer-assisted image quantification system by Image-Pro Plus software.

Statistical analysis

Data are presented as the mean ± standard deviation, and all cell culture experiments were conducted in three independent experiments. Histological and IHC staining were assessed by a single observer blinded to treatment. For quantitative analysis, five random fields from two sections per mouse were selected and imaged on a Nikon microscope, and images were analyzed with Image-Pro Plus Software. Differences between the two groups were analyzed using unpaired Student's t test, and one-way ANOVA analysis with Tukey's post-test was used for multiple comparisons. Repeated measures data were evaluated using repeated measures ANOVA. Differences with $p < 0.05$ were considered statistically significant.

RESULTS

MK2206 attenuated atherosclerosis in ApoE$^{-/-}$ mice

The incidence of atherosclerosis increases with age, and patients with such disorders usually have accompanying tumorigenesis. To explore the role of the anticancer drug MK2206 on atherosclerosis, we constructed a diet-induced atherosclerosis model using ApoE$^{-/-}$ mice (Fig. 1a). After 8 weeks of treatment, the mice were euthanized, and lipid accumulation was measured by ORO staining assay. Compared with the HFD group, MK2206 significantly diminished lipid accumulation (Fig. 1b, c, Supplementary Fig. 1a, b). Furthermore, we have selected three markers of inflammation in the vascular lesions. Fragments of oxLDL are taken up by SR-A binding to MHC-II molecules, and the complexes are recognized by CD4$^+$ T cells, stimulating cytokine secretion [35, 36]. Mac-3 is a marker for macrophages that has been used as an indicator for lesion inflammation in atherosclerosis [37]. CCL2 is a key driver of monocyte recruitment and a mediator of intimal hyperplasia in response to arterial injury [38–41]. Thus, we studied the expression of MHC-II, Mac-3, and CCL2 by immunohistochemistry staining, as the indicators of inflammation in the vasculature. We found that the expression of MHC-II (Fig. 1d, e), Mac-3 (Fig. 1f, g), and CCL2 (Fig. 1h, i) was decreased in the MK2206-treatment group compared to the HFD group. In addition, MK2206 had no effect on necrotic core area and fibrous cap area in lesion of the aortic root (Supplementary Fig. 1c–e), and MK2206 inhibited smooth muscle cell proliferation in the arch

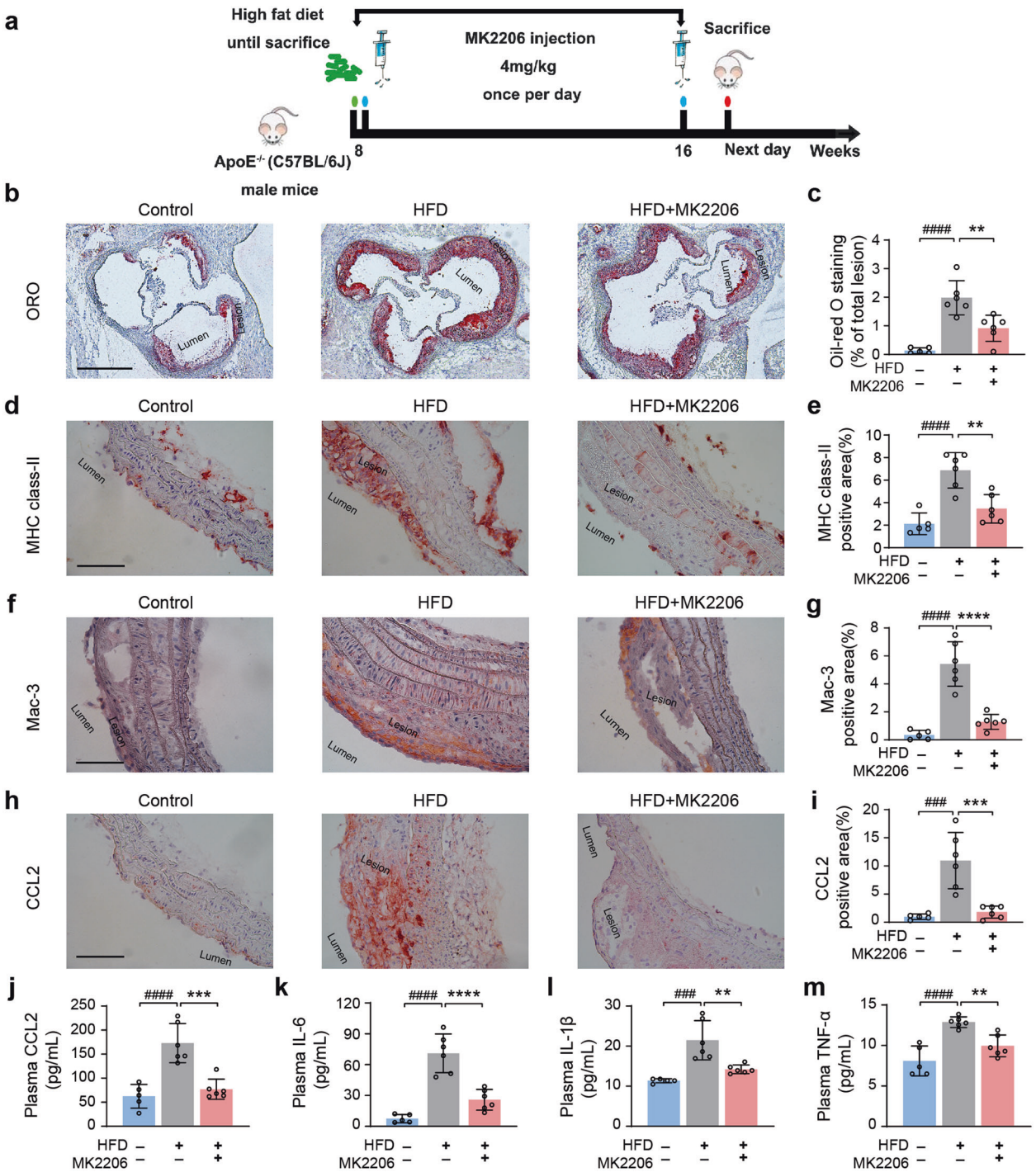

Fig. 1 MK2206 attenuated atherosclerosis in ApoE$^{-/-}$ mice. (**a**) Schematic diagram of experimental animal model and treatment administration. Representative images of Oil Red O staining (×50) of the aortic root (**b**) and the associated quantitative analysis (**c**). Representative immunohistochemical staining images (×400) of MHC-II (**d**), Mac-3 (**f**), and CCL2 (**h**) in the aortic arch, and the related quantitative analysis, respectively (**e**, **g**, **i**). (**j**–**m**) Plasma CCL2, IL-6, IL-1β, and TNF-α of ApoE$^{-/-}$ mice from control, HFD, and HFD + MK2206 groups were detected by ELISA, respectively. Data are presented as the mean ± standard deviation. $^{**}P < 0.01$, $^{***}P < 0.001$, $^{****}P < 0.0001$ vs. the model group (high-fat diet group), $^{\#\#\#}P < 0.001$, $^{\#\#\#\#}P < 0.0001$ vs. the control group (normal chow diet group). Scale bar: **b** = 500 μm; **d**, **f**, **h** = 50 μm.

(Supplementary Fig. 1f, g). We further measured the plasma levels of inflammatory cytokines, including CCL2, IL-6, IL-1β, and TNF-α. These cytokines were all decreased by the treatment with MK2206, compared to the HFD group (Fig. 1j–m). Taken together, these findings illustrated that MK2206 mitigated atherosclerosis in ApoE$^{-/-}$ mice by attenuating inflammatory response, VSMC proliferation, and lipid deposition, without influence on the stability of plaque.

Effects of MK2206 on cell viability and Akt activity

It is well known that macrophages, smooth muscle, and endothelial cells participate in the pathological progress of

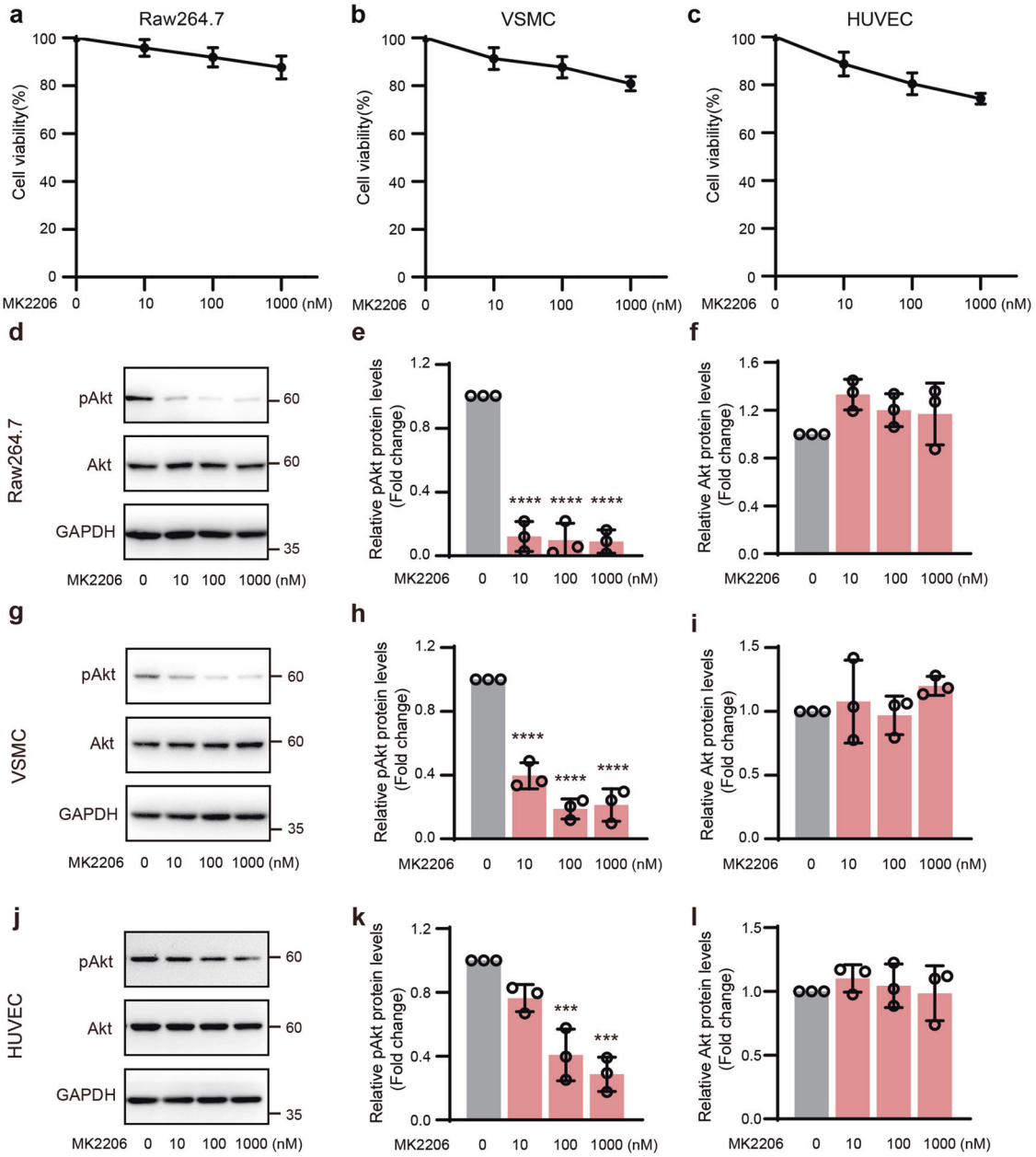

Fig. 2 Cell viability assay and Akt activity in response to MK2206. (**a**–**c**) Raw264.7, VSMC, and HUVEC cells were treated with MK2206 in a dose-dependent manner for 24 h, and CCK-8 assay was applied to detect cell viability. Representative immunoblot images (**d**, **g**, **j**) and quantification of pAkt (**e**, **h**, **k**) and Akt (**f**, **i**, **l**) in Raw264.7, VSMC, and HUVEC cells, respectively. Data are presented as the mean ± standard deviation from three independent experiments. ***$P < 0.001$, ****$P < 0.0001$ vs. the control group (0 nM group).

vascular injury in atherosclerosis. To further evaluate the molecular mechanism of MK2206 in preventing atherosclerotic lesion formation, we first measured the cytotoxicity of MK2206 on the three cell types above to determine an effective and safe dose. Different concentrations (10, 100, 1000 nM) of MK2206 had no significant effect on Raw264.7, VSMC, and HUVEC cell viability (Fig. 2a–c). Meanwhile, we also detected the activity of Akt and its downstream mediator mTOR in Raw264.7, VSMC, and HUVEC cells, after MK2206 stimulation. Result showed that the phosphorylation of Akt (Fig. 2d–l) and mTOR (Supplementary Fig. 2) were significantly dampened by MK2206. Based on MK2206 cytotoxicity and efficacy tests in these three cell lines, 100 nM dose was used for all subsequent in vitro experiments.

MK2206 inhibited macrophage-derived foam cell formation and inflammatory response

Macrophage-derived foam cells formation represents a key factor in the initiation of atherosclerosis [15, 42]. Previous studies suggest that Akt-dependent signaling pathways are involved in foam cell formation and atherosclerosis [43, 44], while Akt deficiency in macrophages impedes atherosclerosis progression [30, 45]. To investigate whether inhibition of Akt activity could reduce foam cell formation, oxLDL-stimulated Raw264.7 cells were treated with Akt specific inhibitor, MK2206, and lipid deposition was detected by ORO staining. As shown in Fig. 3a, b, lipid area and foam cell formation were significantly decreased by MK2206 in a dose-dependent manner. Lipid deposition in cells is caused by the

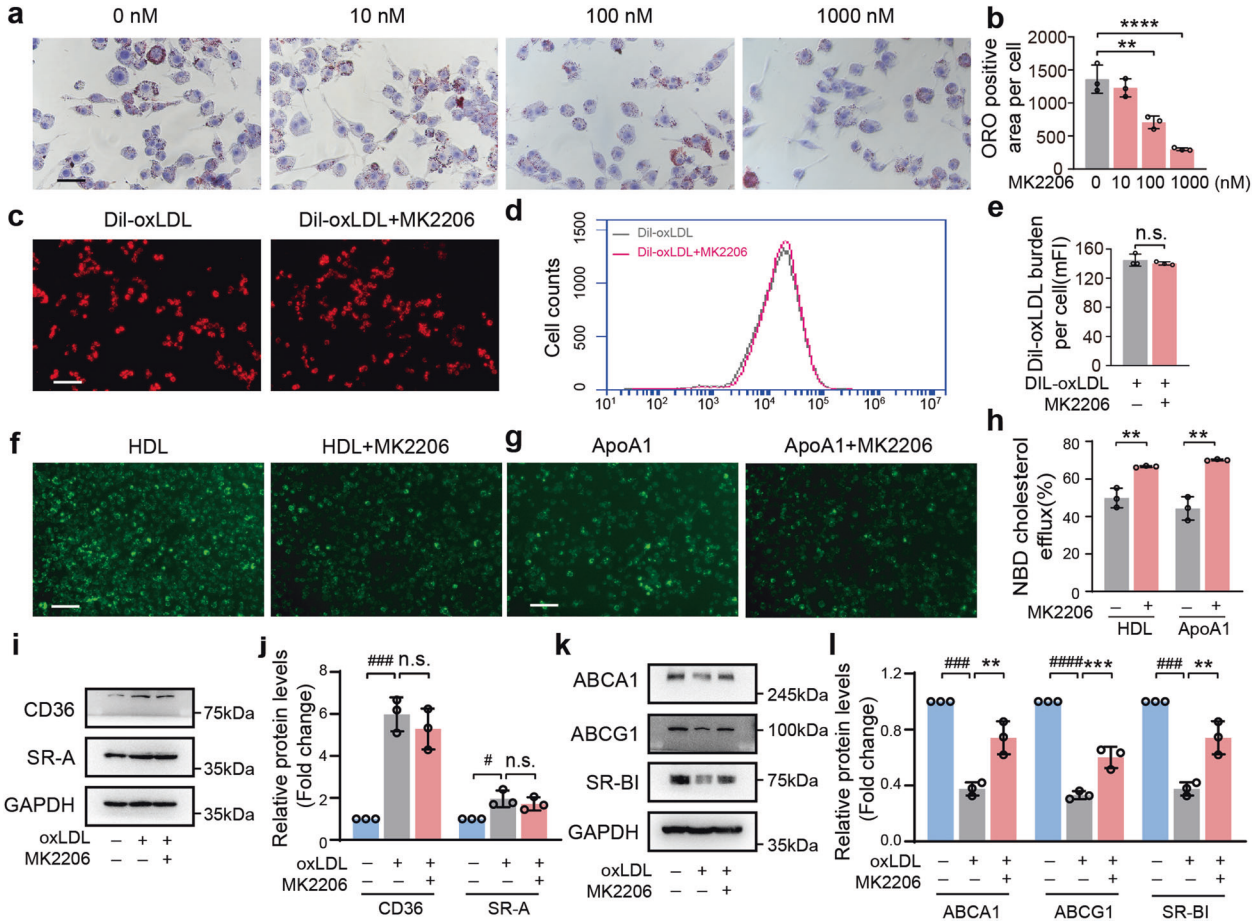

Fig. 3 MK2206 inhibited macrophage-derived foam cell formation. (**a**) Representative ORO images (×400) in the indicated group. Raw264.7 cells were treated with MK2206 at different concentrations for 30 min, before stimulated with oxLDL for 24 h. (**b**) The average ORO area per cell was assessed as a result of a numerical average of positive area in the individual cell per field. (**c**) Representative fluorescence images (×200) of Raw264.7 cells labeled with Dil-oxLDL for 6 h. (**d**) Representative flow cytometry plot of Dil-oxLDL-processed Raw264.7 cells and (**e**) quantification of mean Dil-oxLDL burden (MFI). Representative fluorescence images (×200) of NBD-cholesterol-loaded Raw264.7 cells after incubated with HDL (**f**) or ApoA1 (**g**) for 4 h, and the percentage of cholesterol efflux mediated by HDL and ApoA1 (**h**). Representative immunoblot images (**i**) and quantification (**j**) of CD36 and SR-A in Raw264.7 cells treated with oxLDL and MK2206 for 24 h. Representative immunoblot images (**k**) and quantification (**l**) of ABCA1, ABCG1, and SR-BI in Raw264.7 cells treated with oxLDL and MK2206 for 24 h. Data are presented as the mean ± standard deviation from three independent experiments. $^{**}P < 0.01$, $^{***}P < 0.001$, $^{****}P < 0.0001$ vs. the model group (oxLDL or Dil-oxLDL-treated group), $^{\#\#\#}P < 0.001$, $^{\#\#\#\#}P < 0.0001$ vs. the control group (no treatment group), n.s. indicated the data meant no statistical difference. Scale bar: **a** = 100 μm, **c**, **f**, **g** = 50 μm.

increased lipid uptake or decreased cholesterol efflux [46]. Hence, we used Dil-oxLDL uptake assay and NBD-cholesterol efflux assay to evaluate oxLDL phagocytosis and cholesterol efflux after cells were treated with MK2206. Phagocytosis of Dil-oxLDL in Raw264.7 cells was not affected by MK2206, as analyzed by immunofluorescent staining and flow cytometry assay (Fig. 3c–e). Meanwhile, compared with oxLDL-treated cells, the mRNA (Supplementary Fig. 3a) and protein (Fig. 3i, j) levels of scavenger receptors, CD36 and SR-A, which mediated phagocytosis in Raw264.7 cells, showed no significant changes after MK2206 treatment. Subsequently, we assessed whether MK2206 blocks the efflux of cholesterol in Raw264.7 cells. ApoA1 and HDL were supplemented to cells to induce cholesterol efflux in NBD-cholesterol-loaded cells treated with MK2206. We found that cholesterol efflux either to ApoA1 or HDL was significantly increased after MK2206 treatment (Fig. 3f–h). To further confirm our findings, we detected the mRNA (Supplementary Fig. 3b) and protein (Fig. 3k, l) levels of cholesterol transporters, ABCA1, ABCG1, and SR-BI, which mediated cholesterol efflux. The results showed that the expression levels were elevated in MK2206 and oxLDL-treated cells, compared with oxLDL-treated cells alone. The results above demonstrated that MK2206 inhibited macrophage-derived foam cell formation by promoting cholesterol efflux but did not impact lipid uptake.

In addition to lipid accumulation, chronic inflammation also accelerates atherosclerotic plaque formation [47]. Hence, we investigated the effects of MK2206 on LPS or oxLDL-induced proatherogenic cytokines expression in Raw264.7 cells. MK2206 markedly reduced the level of CCL2 (Fig. 4a), IL-6 (Fig. 4d), IL-1β (Fig. 4g), and TNF-α (Fig. 4j) mRNA expression induced by LPS in macrophages, similar results were obtained in oxLDL-induced inflammatory experiment in macrophages (Supplementary Fig. 3c–f). We next investigated the mechanisms driving a decreased inflammatory response in MK2206-treated cells. We used actinomycin D to inhibit gene transcription and found that the half-lives of inflammatory cytokine were shorter in the presence of MK2206 in Raw264.7 cells (Fig. 4b, e, h, k). Consistently, the level of these proinflammatory factors in cell supernatants was decreased by MK2206 as measured by ELISA assay (Fig. 4c, f, i, l and Supplementary Fig. 3g–j). Based on these results, we confirmed that MK2206 reduces either LPS-induced or oxLDL-induced inflammatory response in Raw264.7 cells, and this process was regulated by the mRNA stability of associated cytokines. In addition, macrophages secrete high levels of MMPs that facilitate VSMC migration and

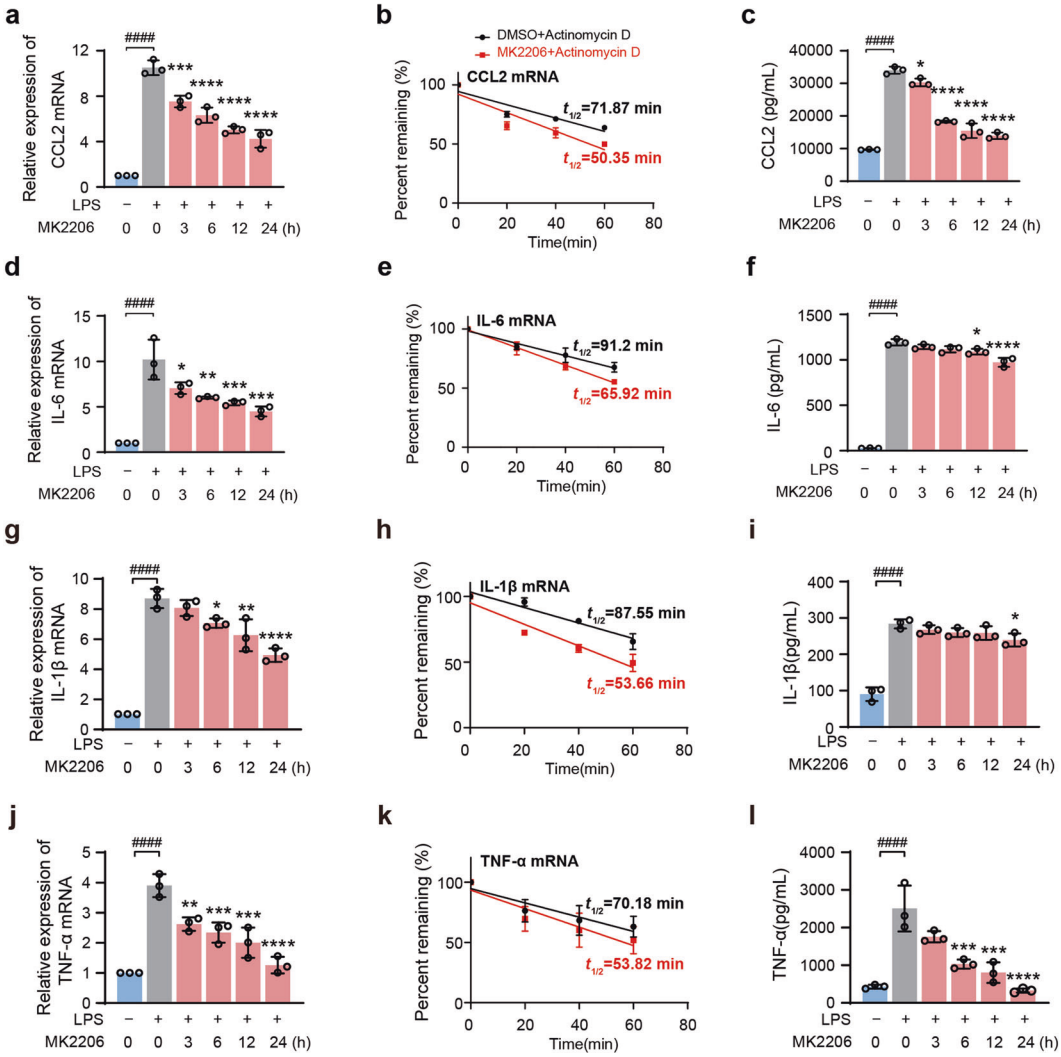

Fig. 4 MK2206 inhibited inflammation in macrophages. Relative expression of CCL2-mRNA (**a**), IL-6-mRNA (**d**), IL-1β-mRNA (**g**), and TNF-α-mRNA (**j**) in Raw264.7 cells, and levels of CCL2 (**c**), IL-6 (**f**), IL-1β (**i**), and TNF-α (**l**) in supernatants after stimulation with LPS and MK2206 for different lengths of time. (**b**, **e**, **h**, **k**) The half-lives of CCL2, IL-6, IL-1β, and TNF-α were decreased after Raw264.7 cells were incubated with MK2206. Data are presented as the mean ± standard deviation from three independent experiments. $^{*}P < 0.05$, $^{**}P < 0.01$, $^{***}P < 0.001$, $^{****}P < 0.0001$ vs. the model group (LPS treated group), $^{\#\#\#\#}P < 0.0001$ vs. the control group (no treatment group).

proliferation, we found that MK2206 also decreased macrophage proliferation (Supplementary Fig. 3k) and MMP9 and MMP2 levels (Supplementary Fig. 3l–n), these results suggested that MK2206 reduced the levels of macrophage-derived MMPs, which might affect VSMC migration and proliferation.

MK2206 inhibited migration, proliferation, and inflammation in VSMCs

PDGF-BB induces proliferation and migration of VSMC contributing to the progression of atherosclerosis [48, 49]. Moreover, Akt-dependent signaling pathways have been involved in cell migration and cell proliferation [50, 51]. The result of animal experiment above suggested that MK2206 might decrease VSMC proliferation. To test whether reducing Akt activity could inhibit VSMC migration and proliferation in vitro, PDGF-BB-stimulated VSMCs were treated with MK2206. VSMC migration was detected by transwell (Fig. 5a, b) and wound healing assays (Fig. 5c, d), the results showed that MK2206 inhibited VSMC migration. Besides, VSMC proliferation was more effectively suppressed by MK2206 treatment (Fig. 5e). In addition, the mRNA (Supplementary Fig. 4) and protein (Fig. 5f, g) levels of MMP9 and MMP2, which facilitate matrix remodeling, VSMC migration, and proliferation [52], were also decreased by the treatment with MK2206. Therefore, MK2206 could alleviate atherosclerosis progress by inhibiting VSMC migration and proliferation.

In addition, we also measured the inflammatory response in VSMCs after treatment with MK2206. The results were consistent with Raw264.7 cell experiments, where CCL2 (Fig. 5h, j) and IL-6 expression (Fig. 5k, m) were decreased by promoting mRNA decay (Fig. 5i, l). Therefore, MK2206 inhibited migration, proliferation, and inflammation in VSMCs.

MK2206 inhibited proliferation and inflammation in HUVECs

Besides macrophages and VSMCs, inflammation and proliferation in endothelial cells also play important roles in atherogenesis [53]. We also assessed the proliferative and inflammatory response in HUVECs after treatment with MK2206. As shown in Fig. 6, MK2206 markedly reduced CCL2 (Fig. 6a, c) and IL-6 expression (Fig. 6d, f) by affecting mRNA stability (Fig. 6b, e), and decreased the mRNA expression of ICAM1, VCAM1, E-selectin, and P-selectin (Fig. 6g, h, j, k). IL-8 mRNA levels showed a decreasing trend but did not achieve statistical significance (Fig. 6i). In addition, proliferation of HUVECs was inhibited by the treatment with MK2206 (Fig. 6l).

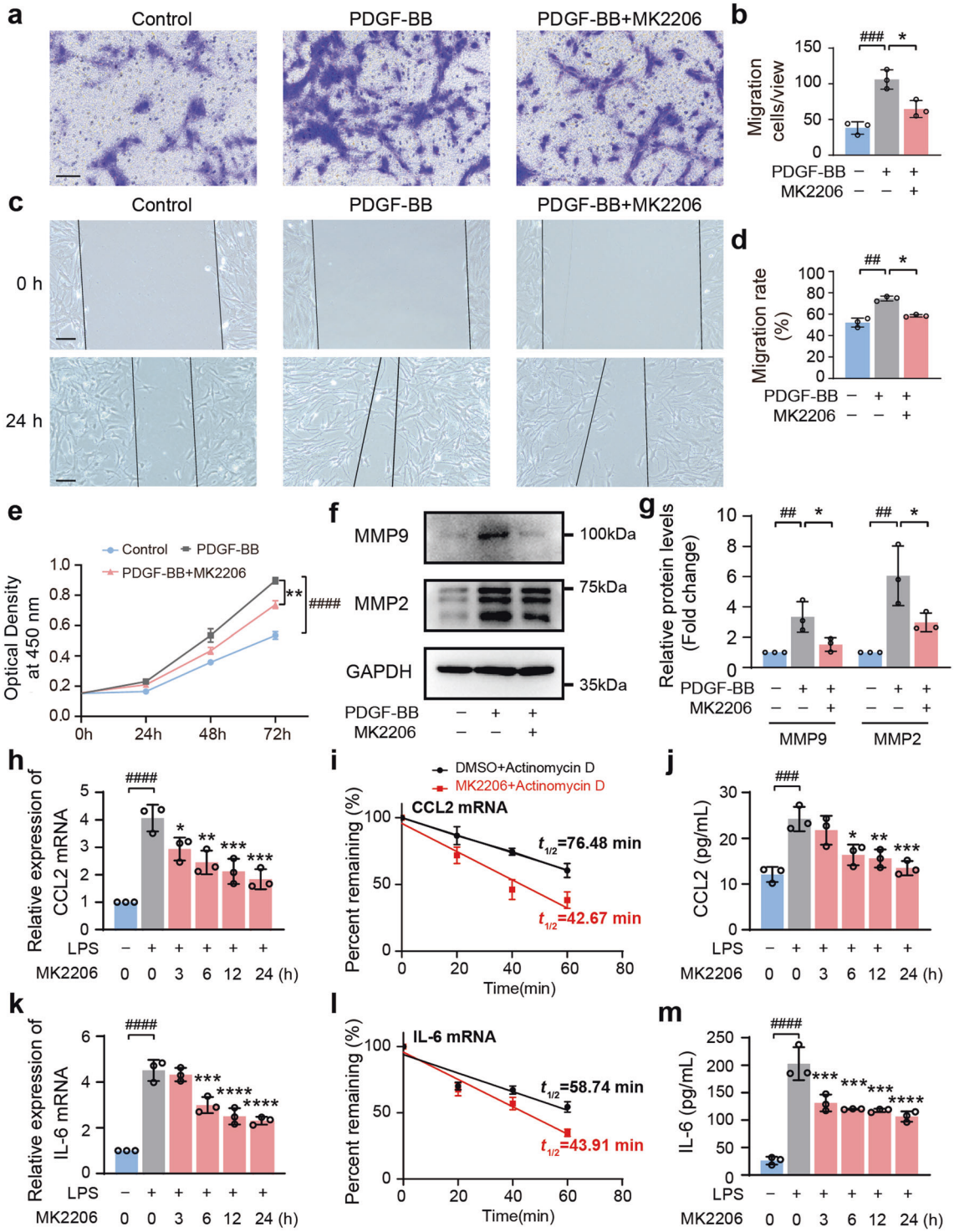

Fig. 5 MK2206 inhibited migration, proliferation, and inflammation in VSMCs. VSMC migration was analyzed by transwell (**a**, crystal violet stain, ×200) and wound healing (**c**, ×100) assays. Migration was presented as migrated cells per view (**b**) and migration rate (**d**). (**e**) Proliferation of VSMCs was assessed by CCK-8 assay. Representative immunoblot images (**f**) and quantification (**g**) of MMP9 and MMP2 expression. Relative expression of CCL2-mRNA (**h**) and IL-6-mRNA (**k**) in VSMCs and levels of CCL2 (**j**) and IL-6 (**m**) in supernatants after stimulation with LPS and MK2206. (**i**, **l**) The half-lives of CCL2 and IL-6 were decreased after VSMCs were incubated with MK2206. Data are presented as the mean ± standard deviation from three independent experiments. $^{*}P < 0.05$, $^{**}P < 0.01$, $^{***}P < 0.001$, $^{****}P < 0.0001$ vs. the model group (PDGF-BB or LPS treated group), $^{\#\#}P < 0.01$, $^{\#\#\#}P < 0.001$, $^{\#\#\#\#}P < 0.0001$ vs. the control group (no treatment group). Scale bar: **a** = 50 μm, **c** = 100 μm.

DISCUSSION

In this study, we demonstrated beneficial effects of the antitumor drug MK2206 on the cardiovascular system. Our findings showed that MK2206 effectively attenuated atherosclerosis and protected against vascular toxicity in vivo. Also, MK2206 decreased lipid accumulation in macrophages by promoting cholesterol efflux. In parallel, we have revealed that MK2206 could reduce VSMC migration, decrease the proliferation of Raw264.7, VSMC, and

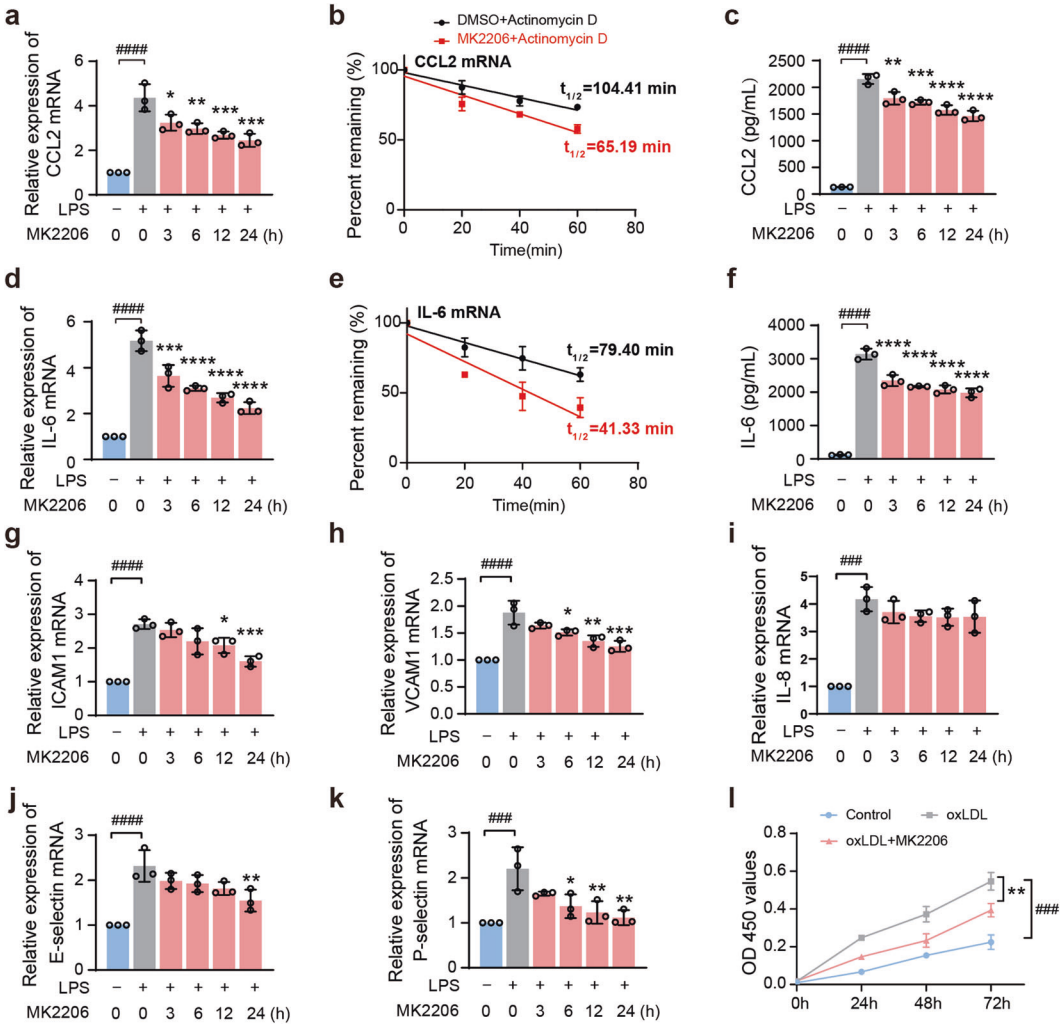

Fig. 6 MK2206 reduced the inflammatory response in HUVECs. Relative expression of CCL2-mRNA (**a**) and IL-6-mRNA (**d**) in HUVECs and levels of CCL2 (**c**) and IL-6 (**f**) in supernatants after stimulation with LPS and MK2206 for different lengths of time. (**b**, **e**) The half-lives of CCL2 and IL-6 were decreased after HUVECs were incubated with MK2206. Relative mRNA expression of ICAM1 (**g**), VCAM1 (**h**), IL-8 (**i**), E-selectin (**j**), and P-selectin (**k**). (**l**) Proliferation of HUVECs was assessed by CCK-8 assay. Data are presented as the mean ± standard deviation from three independent experiments. $^{*}P < 0.05$, $^{**}P < 0.01$, $^{***}P < 0.001$, $^{****}P < 0.0001$ vs. the model group (LPS or oxLDL-treated group), $^{\#\#\#}P < 0.001$, $^{\#\#\#\#}P < 0.0001$ vs. the control group (no treatment group).

HUVEC cells, and alleviate inflammatory responses in macrophages, VSMC, and endothelial cells. The results together indicated that MK2206 exerted a protective effect on the cardiovascular system.

MK2206 is a small molecule allosteric AKT inhibitor, showing promising results in antitumor therapy clinical trials [54]. However, few studies have focused on the effect of MK2206 on the cardiovascular system. Studies showed that MK2206 inhibited the proliferation of endothelial cells induced by oxLDL [55], and reversed the promoting effect of VSMC proliferation and migration mediated by miR-21 overexpression [56]. In agreement with these reports, we demonstrated that MK2206 suppressed proliferation of Raw264.7, VSMC, and HUVEC cells, and it also inhibited VSMC migration. However, we found that MK2206 had no effect on necrotic core area and fibrous cap area, which are associated with the stability of vulnerable plaques. These results suggested that MK2206 predominantly plays a role in early atherosclerosis. In addition, Marshall et al. [57] revealed that MK2206 reversed the reduction of cholesterol efflux mediated by free fatty acid in macrophage, and Pi et al. [58] reported that MK2206 abolished lipid accumulation and cholesterol efflux induced by ADPβ (a P2RY12 receptor activator) in VSMCs. These research findings also support our results demonstrating that MK2206 decreased lipid deposition induced by oxLDL in macrophages, and that this process was associated with the increase of cholesterol efflux but not lipid uptake. Furthermore, this observation was corroborated in vivo. In addition, we also revealed that MK2206 reduced inflammatory response in vitro and in vivo, by mediating the mRNA decay of inflammatory factors. Therefore, our results suggested that MK2206 had a protective effect against atherosclerosis.

In this study, we found that MK2206 reduced macrophage lipid accumulation, VSMCs migration, and proliferation of Raw264.7, VSMC, and HUVEC cells. Interestingly, it also decreased the inflammatory response in atherosclerosis. These beneficial effects might be related to the differential physiological functions of each Akt isoform. Previous studies revealed that Akt2 predominantly affects macrophage migration, inflammation, and lipid deposition [59], and hematopoietic cell Akt2 deficiency exhibited less atherosclerosis in Ldl receptor-Null ($Ldlr^{-/-}$) mice [30, 45, 60]. Hence, the reduction of lipid deposition and inflammation mediated by MK2206 could be attributed to the decreased activity of Akt2. In addition, Akt1 inhibition decreases VSMC migration and survival [61, 62], and also induce macrophage

apoptosis [63, 64]. In our study, we found that MK2206 showed antimigrative and antiproliferative effects on VSMCs, which might be ascribed to the decrease of Akt1 activity. As inhibition of VSMC migration and proliferation could reduce plaque formation at the early stage of atherosclerosis, MK2206 showed an antiatherosclerosis effect at least in early atherosclerosis.

Akt is an upstream regulator of mTOR, while mTOR has been reported to be involved in many CVDs, including atherosclerosis [65, 66]. Inhibition of mTOR limits atherosclerosis by reducing proliferation and migration of VSMCs, enhancing autophagy of macrophages and decreasing their accumulation [67], and inhibiting foam cell formation in the plaque [66]. As inhibitors of mTOR, rapamycin has been reported to be effective against atherosclerosis in ApoE$^{-/-}$ mice by attenuating inflammation [68], promoting cholesterol efflux [69], and enhancing the stability of atherosclerotic plaques [67]. In a number of previous studies, targeting Akt/mTOR signaling has been reported to be effective in alleviating atherosclerosis [70–73]. Here, we have demonstrated that MK2206, a specific inhibitor of Akt, inhibited the phosphorylation of mTOR, and decreased VSMC migration and proliferation, suppressed foam cell formation, and reduced the inflammatory response in ApoE$^{-/-}$ mice. The results suggested that the effects of MK2206 in atherosclerosis could be attributed to the inhibition of the Akt/mTOR pathway. In addition, Akt phosphorylates many downstream substrates [74], in the study of mechanisms mediating the decreased inflammatory response in MK2206-treated cells, we demonstrated that MK2206 promoted mRNA decay of cytokines. Akt can directly activate Y box-binding protein-1 (YB1) [75], which affects inflammatory response by the regulation of mRNA stability [76, 77]. Taken together, the reports above and our findings suggest that the anti-inflammatory effects of MK2206 might be attributed to the inhibition of YB1, resulting in rapid mRNA decay of cytokines. A limitation of this study is that we did not explore the further molecular mechanisms of MK2206 behind these results. We will continue to reveal the specific roles and mechanisms of MK2206 on CVDs in future studies.

In conclusion, our study reveals that the Akt inhibitor MK2206 has antiatherogenic effects through the decrease of lipid deposition, cell migration and proliferation, as well as the reduction of inflammation. Overall, this study provides prospective evidence for the prevention of cardiovascular comorbidities in cancer therapy.

ACKNOWLEDGEMENTS

This study was financially supported by the National Key Research and Development Program of China Grants 2019YFA0801700 and 2019YFA0801800 (to JW), National Natural Science Foundation of China Grants 81800359 (to HMZ), Chinese Academy of Medical Sciences Innovation Fund for Medical Sciences (2016-I2M-1-006) (to JW), Peking Union Medical College Youth Fund/Fundamental Research Funds for the Central University (3332016048) (to HMZ), National Key Research and Development program of China, Ministry of Science and Technology of China (2018YFC1315100) to (HMZ), and National Natural Science Foundation of China Grants 81622008 and 81470579 (to JW).

AUTHOR CONTRIBUTIONS

JW and HMZ designed and supervised the research. YQT performed the experiments, analyzed the data, and wrote the paper. HMZ and CG performed some of the experiments. ZWL, CLH, HQY, and YFF contributed to the writing of the paper. PRY, HMZ, and JW contributed to the critical revision of the manuscript. All authors provided final approval of the article.

ADDITIONAL INFORMATION

Supplementary information The online version contains supplementary material available at https://doi.org/10.1038/s41401-021-00729-x.

Competing interests: The authors declare no competing interests.

REFERENCES

1. Fitzmaurice C, Dicker D, Pain A, Hamavid H, Moradi-Lakeh M, MacIntyre MF, et al. The global burden of cancer 2013. JAMA Oncol. 2015;1:505–27.
2. Renzi C, Kaushal A, Emery J, Hamilton W. Comorbid chronic diseases and cancer diagnosis: disease-specific effects and underlying mechanisms. Nat Rev Clin Oncol. 2019;16:746–61.
3. Bertero E, Canepa M, Maack C, Ameri P. Linking heart failure to cancer: background evidence and research perspectives. Circulation. 2018;138:735–42.
4. Bonsu JM, Guha A, Charles L, Yildiz VO, Wei L, Baker B, et al. Reporting of cardiovascular events in clinical trials supporting FDA approval of contemporary cancer therapies. J Am Coll Cardiol. 2020;75:620–8.
5. Armstrong GT, Liu Q, Yasui Y, Neglia JP, Leisenring W, Robison LL, et al. Late mortality among 5-year survivors of childhood cancer: a summary from the Childhood Cancer Survivor Study. J Clin Oncol. 2009;27:2328–38.
6. Herrmann J. Vascular toxic effects of cancer therapies. Nat Rev Cardiol. 2020;17:503–22.
7. Abeyrathna P, Su Y. The critical role of Akt in cardiovascular function. Vasc Pharmacol. 2015;74:38–48.
8. Fruman DA, Chiu H, Hopkins BD, Bagrodia S, Cantley LC, Abraham RT. The PI3K pathway in human disease. Cell. 2017;170:605–35.
9. Jonasch E, Hasanov E, Corn PG, Moss T, Shaw KR, Stovall S, et al. A randomized phase 2 study of MK-2206 versus everolimus in refractory renal cell carcinoma. Ann Oncol. 2017;28:804–8.
10. Oki Y, Fanale M, Romaguera J, Fayad L, Fowler N, Copeland A, et al. Phase II study of an AKT inhibitor MK2206 in patients with relapsed or refractory lymphoma. Br J Haematol. 2015;171:463–70.
11. Lopez-Chavez A, Thomas A, Rajan A, Raffeld M, Morrow B, Kelly R, et al. Molecular profiling and targeted therapy for advanced thoracic malignancies: a biomarker-derived, multiarm, multihistology phase II basket trial. J Clin Oncol. 2015;33:1000–7.
12. Cheng GZ, Park S, Shu S, He L, Kong W, Zhang W, et al. Advances of AKT pathway in human oncogenesis and as a target for anti-cancer drug discovery. Curr Cancer Drug Targets. 2008;8:2–6.
13. Benjamin EJ, Blaha MJ, Chiuve SE, Cushman M, Das SR, Deo R, et al. Heart Disease and Stroke Statistics-2017 update: a report from the American Heart Association. Circulation. 2017;135:e146–603.
14. Fichtlscherer S, Breuer S, Zeiher AM. Prognostic value of systemic endothelial dysfunction in patients with acute coronary syndromes: further evidence for the existence of the "vulnerable" patient. Circulation. 2004;110:1926–32.
15. Libby P. Inflammation in atherosclerosis. Nature. 2002;420:868–74.
16. Basatemur GL, Jørgensen HF. Vascular smooth muscle cells in atherosclerosis. Nat Rev Cardiol. 2019;16:727–44.
17. Tiwari RL, Singh V, Barthwal MK. Macrophages: an elusive yet emerging therapeutic target of atherosclerosis. Med Res Rev. 2008;28:483–544.
18. Yvan-Charvet L, Wang N, Tall AR. Role of HDL, ABCA1, and ABCG1 transporters in cholesterol efflux and immune responses. Arterioscler Thromb Vasc Biol. 2010;30:139–43.
19. Martinez LO, Jacquet S, Esteve JP, Rolland C, Cabezón E, Champagne E, et al. Ectopic beta-chain of ATP synthase is an apolipoprotein A-I receptor in hepatic HDL endocytosis. Nature. 2003;421:75–9.
20. Visse R, Nagase H. Matrix metalloproteinases and tissue inhibitors of metalloproteinases: structure, function, and biochemistry. Circ Res. 2003;92:827–39.
21. Sternlicht MD, Werb Z. How matrix metalloproteinases regulate cell behavior. Annu Rev Cell Dev Biol. 2001;17:463–516.
22. Lin J, Kakkar V, Lu X. Impact of matrix metalloproteinases on atherosclerosis. Curr Drug Targets. 2014;15:442–53.
23. Bevilacqua MP, Stengelin S, Gimbrone MA Jr, Seed B. Endothelial leukocyte adhesion molecule 1: an inducible receptor for neutrophils related to complement regulatory proteins and lectins. Science. 1989;243:1160–5.
24. Nourshargh S, Alon R. Leukocyte migration into inflamed tissues. Immunity. 2014;41:694–707.
25. Abbate A, Toldo S, Marchetti C, Kron J, Van Tassell BW, Dinarello CA. Interleukin-1 and the inflammasome as therapeutic targets in cardiovascular disease. Circ Res. 2020;126:1260–80.
26. Klingenberg R, Hansson GK. Treating inflammation in atherosclerotic cardiovascular disease: emerging therapies. Eur Heart J. 2009;30:2838–44.
27. Koenen RR, Weber C. Therapeutic targeting of chemokine interactions in atherosclerosis. Nat Rev Drug Discov. 2010;9:141–53.
28. Bandaru S, Ala C, Salimi R, Akula MK, Ekstrand M, Devarakonda S, et al. Targeting filamin A reduces macrophage activity and atherosclerosis. Circulation. 2019;140:67–79.
29. Rotllan N, Wanschel AC, Fernández-Hernando A, Salerno AG, Offermanns S, Sessa WC, et al. Genetic evidence supports a major role for Akt1 in VSMCs during atherogenesis. Circ Res. 2015;116:1744–52.

30. Rotllan N, Chamorro-Jorganes A, Araldi E, Wanschel AC, Aryal B, Aranda JF, et al. Hematopoietic Akt2 deficiency attenuates the progression of atherosclerosis. FASEB J. 2015;29:597–610.
31. Rousselle A, Qadri F, Leukel L, Yilmaz R, Fontaine JF, Sihn G, et al. CXCL5 limits macrophage foam cell formation in atherosclerosis. J Clin Invest. 2013;123:1343–7.
32. Fang L, Choi SH, Baek JS, Liu C, Almazan F, Ulrich F, et al. Control of angiogenesis by AIBP-mediated cholesterol efflux. Nature. 2013;498:118–22.
33. Wang J, Chong KK, Nakamura Y, Nguyen L, Huang SK, Kuo C, et al. B7-H3 associated with tumor progression and epigenetic regulatory activity in cutaneous melanoma. J Invest Dermatol. 2013;133:2050–8.
34. Chen Y, Duan Y, Yang X, Sun L, Liu M, Wang Q, et al. Inhibition of ERK1/2 and activation of LXR synergistically reduce atherosclerotic lesions in ApoE-deficient mice. Arterioscler Thromb Vasc Biol. 2015;35:948–59.
35. Nicoletti A, Caligiuri G, Törnberg I, Kodama T, Stemme S, Hansson GK. The macrophage scavenger receptor type A directs modified proteins to antigen presentation. Eur J Immunol. 1999;29:512–21.
36. Virella G, Lopes-Virella MF. Atherogenesis and the humoral immune response to modified lipoproteins. Atherosclerosis. 2008;200:239–46.
37. Zhang X, Li J, Luo S, Wang M, Huang Q, Deng Z, et al. IgE contributes to atherosclerosis and obesity by affecting macrophage polarization, macrophage protein network, and foam cell formation. Arterioscler Thromb Vasc Biol. 2020;40:597–610.
38. Aiello RJ, Bourassa PA, Lindsey S, Weng W, Natoli E, Rollins BJ, et al. Monocyte chemoattractant protein-1 accelerates atherosclerosis in apolipoprotein E-deficient mice. Arterioscler Thromb Vasc Biol. 1999;19:1518–25.
39. Boring L, Gosling J, Cleary M, Charo IF. Decreased lesion formation in CCR2-/- mice reveals a role for chemokines in the initiation of atherosclerosis. Nature. 1998;394:894–7.
40. Gosling J, Slaymaker S, Gu L, Tseng S, Zlot CH, Young SG, et al. MCP-1 deficiency reduces susceptibility to atherosclerosis in mice that overexpress human apolipoprotein B. J Clin Invest. 1999;103:773–8.
41. Gu L, Okada Y, Clinton SK, Gerard C, Sukhova GK, Libby P, et al. Absence of monocyte chemoattractant protein-1 reduces atherosclerosis in low density lipoprotein receptor-deficient mice. Mol Cell. 1998;2:275–81.
42. Lusis AJ. Atherosclerosis. Nature. 2000;407:233–41.
43. Zhou M, Ren P, Zhang Y, Li S, Li M, Li P, et al. Shen-Yuan-Dan capsule attenuates atherosclerosis and foam cell formation by enhancing autophagy and inhibiting the PI3K/Akt/mTORC1 signaling pathway. Front Pharmacol. 2019;10:603.
44. Wang Z, Bao Z, Ding Y, Xu S, Du R, Yan J, et al. Nε-carboxymethyl-lysine-induced PI3K/Akt signaling inhibition promotes foam cell apoptosis and atherosclerosis progression. Biomed Pharmacother. 2019;115:108880.
45. Babaev VR, Hebron KE, Wiese CB, Toth CL, Ding L, Zhang Y, et al. Macrophage deficiency of Akt2 reduces atherosclerosis in Ldlr null mice. J Lipid Res. 2014;55:2296–308.
46. Li AC, Glass CK. The macrophage foam cell as a target for therapeutic intervention. Nat Med. 2002;8:1235–42.
47. Ridker PM, Libby P, MacFadyen JG, Thuren T, Ballantyne C, Fonseca F, et al. Modulation of the interleukin-6 signalling pathway and incidence rates of atherosclerotic events and all-cause mortality: analyses from the Canakinumab Anti-Inflammatory Thrombosis Outcomes Study (CANTOS). Eur Heart J. 2018;39:3499–507.
48. Wang L, Zheng J, Bai X, Liu B, Liu CJ, Xu Q, et al. ADAMTS-7 mediates vascular smooth muscle cell migration and neointima formation in balloon-injured rat arteries. Circ Res. 2009;104:688–98.
49. Raines EW. PDGF and cardiovascular disease. Cytokine Growth Factor Rev. 2004;15:237–54.
50. Alzahrani AS. PI3K/Akt/mTOR inhibitors in cancer: at the bench and bedside. Semin Cancer Biol. 2019;59:125–32.
51. Jabbarzadeh Kaboli P, Salimian F, Aghapour S, Xiang S, Zhao Q, Li M, et al. Akt-targeted therapy as a promising strategy to overcome drug resistance in breast cancer—a comprehensive review from chemotherapy to immunotherapy. Pharmacol Res. 2020;156:104806.
52. Sluijter JP, de Kleijn DP, Pasterkamp G. Vascular remodeling and protease inhibition–bench to bedside. Cardiovasc Res. 2006;69:595–603.
53. Sun HJ, Wu ZY, Nie XW, Bian JS. Role of endothelial dysfunction in cardiovascular diseases: the link between inflammation and hydrogen sulfide. Front Pharmacol. 2019;10:1568.
54. Yap TA, Yan L, Patnaik A, Fearen I, Olmos D, Papadopoulos K, et al. First-in-man clinical trial of the oral pan-AKT inhibitor MK-2206 in patients with advanced solid tumors. J Clin Oncol. 2011;29:4688–95.
55. Zhang C, Adamos C, Oh MJ, Baruah J, Ayee MAA, Mehta D, et al. oxLDL induces endothelial cell proliferation via Rho/ROCK/Akt/p27(kip1) signaling: opposite effects of oxLDL and cholesterol loading. Am J Physiol Cell Physiol. 2017;313:C340–51.
56. Sun P, Tang LN, Li GZ, Xu ZL, Xu QH, Wang M, et al. Effects of MiR-21 on the proliferation and migration of vascular smooth muscle cells in rats with atherosclerosis via the Akt/ERK signaling pathway. Eur Rev Med Pharmacol Sci. 2019;23:2216–22.
57. Marshall JD, Courage ER, Elliott RF, Fitzpatrick MN, Kim AD, Lopez-Clavijo AF. THP-1 macrophage cholesterol efflux is impaired by palmitoleate through Akt activation. PLoS ONE. 2020;15:e0233180.
58. Pi S, Mao L, Chen J, Shi H, Liu Y, Guo X, et al. The P2RY12 receptor promotes VSMC-derived foam cell formation by inhibiting autophagy in advanced atherosclerosis. Autophagy. 2021;17:980–1000.
59. Linton MF, Moslehi JJ, Babaev VR. Akt signaling in macrophage polarization, survival, and atherosclerosis. Int J Mol Sci. 2019;20:2703.
60. Rensing KL, de Jager SC, Stroes ES, Vos M, Twickler MT, Dallinga-Thie GM, et al. Akt2/LDLr double knockout mice display impaired glucose tolerance and develop more complex atherosclerotic plaques than LDLr knockout mice. Cardiovasc Res. 2014;101:277–87.
61. Fernández-Hernando C, József L, Jenkins D, Di Lorenzo A, Sessa WC. Absence of Akt1 reduces vascular smooth muscle cell migration and survival and induces features of plaque vulnerability and cardiac dysfunction during atherosclerosis. Arterioscler Thromb Vasc Biol. 2009;29:2033–40.
62. Fernández-Hernando C, Ackah E, Yu J, Suárez Y, Murata T, Iwakiri Y, et al. Loss of Akt1 leads to severe atherosclerosis and occlusive coronary artery disease. Cell Metab. 2007;6:446–57.
63. Kockx MM. Apoptosis in the atherosclerotic plaque: quantitative and qualitative aspects. Arterioscler Thromb Vasc Biol. 1998;18:1519–22.
64. Babaev VR, Ding L, Zhang Y, May JM, Lin PC, Fazio S, et al. Macrophage IKKα deficiency suppresses Akt phosphorylation, reduces cell survival, and decreases early atherosclerosis. Arterioscler Thromb Vasc Biol. 2016;36:598–607.
65. Jia G, Aroor AR, Martinez-Lemus LA, Sowers JR. Overnutrition, mTOR signaling, and cardiovascular diseases. Am J Physiol Regul Integr Comp Physiol. 2014;307:R1198–206.
66. Kurdi A, Martinet W, De Meyer GRY. mTOR inhibition and cardiovascular diseases: dyslipidemia and atherosclerosis. Transplantation. 2018;102:S44–6.
67. Martinet W, De Loof H, De Meyer GRY. mTOR inhibition: a promising strategy for stabilization of atherosclerotic plaques. Atherosclerosis. 2014;233:601–7.
68. Chen WQ, Zhong L, Zhang L, Ji XP, Zhang M, Zhao YX, et al. Oral rapamycin attenuates inflammation and enhances stability of atherosclerotic plaques in rabbits independent of serum lipid levels. Br J Pharmacol. 2009;156:941–51.
69. Ou HX, Huang Q, Liu CH, Xiao J, Lv YC, Li X, et al. Midkine inhibits cholesterol efflux by decreasing ATP-binding membrane cassette transport protein A1 via adenosine monophosphate-activated protein kinase/mammalian target of rapamycin signaling in macrophages. Circ J. 2020;84:217–25.
70. Fang S, Wan X, Zou X, Sun S, Hao X, Liang C, et al. Arsenic trioxide induces macrophage autophagy and atheroprotection by regulating ROS-dependent TFEB nuclear translocation and AKT/mTOR pathway. Cell Death Dis. 2021;12:88.
71. Brito PM, Devillard R, Nègre-Salvayre A, Almeida LM, Dinis TC, Salvayre R, et al. Resveratrol inhibits the mTOR mitogenic signaling evoked by oxidized LDL in smooth muscle cells. Atherosclerosis. 2009;205:126–34.
72. Xiong Q, Yan Z, Liang J, Yuan J, Chen X, Zhou L, et al. Polydatin alleviates high-fat diet induced atherosclerosis in apolipoprotein E-deficient mice by autophagic restoration. Phytomedicine. 2021;81:153301.
73. Zhang X, Qin Y, Wan X, Liu H, Lv C, Ruan W, et al. Rosuvastatin exerts anti-atherosclerotic effects by improving macrophage-related foam cell formation and polarization conversion via mediating autophagic activities. J Transl Med. 2021;19:62.
74. Manning BD, Cantley LC. AKT/PKB signaling: navigating downstream. Cell. 2007;129:1261–74.
75. Evdokimova V, Ovchinnikov LP, Sorensen PH. Y-box binding protein 1: providing a new angle on translational regulation. Cell Cycle. 2006;5:1143–7.
76. Lyabin DN, Eliseeva IA, Ovchinnikov LP. YB-1 protein: functions and regulation. Wiley Interdiscip Rev RNA. 2014;5:95–110.
77. Park OH, Park J, Yu M, An HT, Ko J, Kim YK. Identification and molecular characterization of cellular factors required for glucocorticoid receptor-mediated mRNA decay. Genes Dev. 2016;30:2093–105.